


## Quantum capacity analysis of multi-level amplitude damping channels

Stefano Chessa <sup>1</sup>✉ & Vittorio Giovannetti<sup>1</sup>

Evaluating capacities of quantum channels is the first purpose of quantum Shannon theory, but in most cases the task proves to be very hard. Here, we introduce the set of Multi-level Amplitude Damping quantum channels as a generalization of the standard qubit Amplitude Damping Channel to quantum systems of finite dimension  $d$ . In the special case of  $d = 3$ , by exploiting degradability, data-processing inequalities, and channel isomorphism, we compute the associated quantum and private classical capacities for a rather wide class of maps, extending the set of models whose capacity can be computed known so far. We proceed then to the evaluation of the entanglement assisted quantum and classical capacities.

<sup>1</sup>NEST, Scuola Normale Superiore and Istituto Nanoscienze-CNR, Pisa, Italy. ✉email: [stefano.chessa@sns.it](mailto:stefano.chessa@sns.it)

The main goal of quantum information and communication theory is to understand how can we store, process, and transfer information in a reliable way and, from the physical point of view, to individuate realistic platforms by means of which performing these tasks. All this is done by exploiting the characteristic features of quantum mechanics. Focusing on quantum communication, every communication protocol can be seen as a physical system (the encoded message) undergoing some physical transformation that translates it in space or time. Any real-world application though suffers from some kind of noise, each of which can be in turn described as a quantum process or equivalently as a quantum channel. Following the work of Shannon<sup>1</sup> and the later quantum generalizations, the ability of a quantum channel to preserve the encoded classical or quantum information is described by its capacities<sup>2,3</sup>. In the classical case, we can only transfer classical information, hence we only need to deal with the classical capacity. In the quantum framework, we can also transfer quantum states and consequently, in addition to the classical capacity, we count also the quantum capacity. Moreover, the family of capacities associated with a quantum channel can be enlarged assuming the communicating parties to be able to perform specific tasks or to share further resources such as, for instance, entanglement<sup>2,4-8</sup>.

One among the simplest models for quantum noise is given by the amplitude damping channel (ADC). While the ADC has been thoroughly studied and characterized, in terms of capacities in various settings, for the qubit framework<sup>9-12</sup>, a general treatise for qudit ( $d$ -dimensional) systems is still missing and likely not possible to attain. Because of these reasons ADC for  $d > 2$  has to be approached case by case, and the literature regarding capacities of fixed finite dimensions ADC is still remarkably short<sup>12-14</sup>. In recent years though higher dimensional systems have attracted the attention of a growing number of researchers, since they have been shown to provide potential advantages both in terms of computation (see e.g. refs. 15-20) and communication or error correction (see e.g. refs. 21-24) together with the fact that more experimental implementations have been progressively made available (see e.g. refs. 25-32). Both near-term and long-term applications of quantum information, whether in a computational (e.g. distributed quantum computing) or communication (e.g. long-distance quantum communication) framework, will necessitate high-fidelity quantum state transmission to achieve reliable and advantageous purposes. This drives the need of an extensive characterization of communications performances in all available noise regimes and most general noise models. In addition to these considerations, new results on the quantum capacity of finite dimensional channels can also be applied to higher dimensional maps via the partially coherent direct sum (PCDS) channels approach<sup>33</sup>, placing in a wider context the efforts dedicated to the analysis of non-qubit channels. Among non-qubit systems, three-dimensional systems (qutrit) have received particular attention because of their relative accessibility both theoretically and experimentally (see e.g. refs. 34-43).

Considering this, in this paper we focus on the model for quantum noise given by the ADC in the multi-level setting, that we will denote as multi-level amplitude damping (MAD) channel. In particular, we perform a systematic analysis of the MAD on the qutrit space: while we will not approach the issue of the classical capacity of the channel, we will focus on the quantum capacity, private classical capacity, and entanglement-assisted capacities, trying to understand in which conditions these quantities can be known. We find that the quantum and private classical capacities are exactly computable in large regions of the damping parameters space, even when the qutrit MAD are not degradable. When an exact value is missing, we are still able to provide upper bounds exploiting composition rules and data-processing

inequalities. Finally we compute the quantum and classical entanglement-assisted capacities.

## Results and discussion

**MAD channels and composition rules.** The transformations we focus on in the present work are special instances of the multi-level versions of the qubit ADC<sup>9</sup>, hereafter indicated as MAD channels in brief, which effectively describe the decaying of energy levels of a  $d$ -dimensional quantum system A. In its most general form, given  $\{|i\rangle\}_{i=0,\dots,d-1}$  an orthonormal basis of the Hilbert space  $\mathcal{H}_A$  associated with A (hereafter dubbed the computational basis of the problem), a MAD channel  $\mathcal{D}$  is a completely positive trace preserving (CPTP) mapping<sup>2,4-8</sup> acting on the set  $\mathcal{L}(\mathcal{H}_A)$  of linear operators of the system, defined by the following set of  $d(d-1)/2 + 1$  Kraus operators

$$\begin{aligned}\hat{K}_{ij} &\equiv \sqrt{\gamma_{ji}}|i\rangle\langle j|, & \forall i, j \text{ s.t. } 0 \leq i \leq d-1, \\ \hat{K}_0 &\equiv |0\rangle\langle 0| + \sum_{1 \leq j \leq d-1} \sqrt{1-\xi_j}|j\rangle\langle j|,\end{aligned}\quad (1)$$

with  $\gamma_{ji}$  real quantities describing the decay rate from the  $j$ -th to the  $i$ -th level that fulfill the conditions

$$\begin{cases} 0 \leq \gamma_{ji} \leq 1, & \forall i, j \text{ s.t. } 0 \leq i < j \leq d-1, \\ \xi_j \equiv \sum_{0 \leq i < j} \gamma_{ji} \leq 1, & \forall j = 1, \dots, d-1. \end{cases}\quad (2)$$

Accordingly, given  $\hat{\rho} \in \mathfrak{S}(\mathcal{H}_A)$  a generic density matrix of the system A, the MAD channel  $\mathcal{D}$  will transform it into the output state defined as

$$\begin{aligned}\mathcal{D}(\hat{\rho}) &= \hat{K}_0 \hat{\rho} \hat{K}_0^\dagger + \sum_{0 \leq i < j \leq d-1} \hat{K}_{ij} \hat{\rho} \hat{K}_{ij}^\dagger, \\ &= \hat{K}_0 \hat{\rho} \hat{K}_0^\dagger + \sum_{0 \leq i < j \leq d-1} \gamma_{ji} |i\rangle\langle i| \langle j| \hat{\rho} |j\rangle.\end{aligned}\quad (3)$$

By construction,  $\mathcal{D}$  always admits the ground state  $|0\rangle$  as a fixed point, i.e.  $\mathcal{D}(|0\rangle\langle 0|) = |0\rangle\langle 0|$ , even though, depending on the specific values of the coefficients  $\gamma_{ji}$ , other input states may fulfill the same property as well. Limit cases are  $\gamma_{ji} = 0 \forall i, j$ , where all levels are untouched and  $\mathcal{D}$  reduces to the noiseless identity channel  $\text{Id}$  which preserves all the input states of A. On the opposite extreme are those examples in which for some  $j$  we have  $\xi_j = 1$ , corresponding to the scenario where the  $j$ -th level becomes totally depopulated at the end of the transformation. The maps in Eq. (3) provide also a natural playground to describe PCDS channels<sup>33</sup>. Last but not the least, an important and easy to verify property of the maps in Eq. (3) is that they are covariant under the group formed by the unitary transformations  $\hat{U}$  which are diagonal in the computational basis  $\{|i\rangle\}_{i=0,\dots,d-1}$ , i.e.

$$\mathcal{D}(\hat{U} \hat{\rho} \hat{U}^\dagger) = \hat{U} \mathcal{D}(\hat{\rho}) \hat{U}^\dagger, \quad (4)$$

for all inputs  $\hat{\rho}$ .

For what concerns the present work, we shall restrict our analysis to the special set of MAD channels as in Eq. (3) associated with a qutrit system ( $d=3$ ) whose decay processes, pictured in the top panel of Fig. 1, are fully characterized by only three rate parameters  $\gamma_{ji}$  that for the ease of notation we rename with the cartesian components of a 3D vector  $\vec{\gamma} \equiv (\gamma_1, \gamma_2, \gamma_3)$ . Accordingly, expressed in terms of the matrix representation induced by the computational basis  $\{|0\rangle, |1\rangle, |2\rangle\}$ , the Kraus

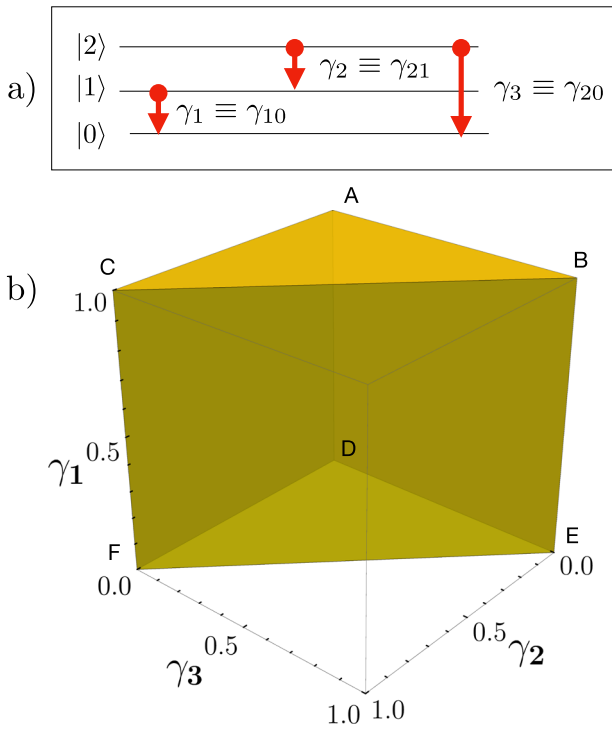


**Fig. 1 Qutrit MAD and parameters region.** **a** Schematic representation of the action of the Multi-level Amplitude Damping (MAD) channel  $\mathcal{D}_{\vec{\gamma}}$  on a three-level system: arrows indicate the damping processes connecting different energy levels (black lines),  $\gamma_{ij}$  are the associated damping parameters. **b** The admitted region of the damping parameters: the transformation is Completely Positive and Trace Preserving (CPTP) if and only if the rate vector  $\vec{\gamma}$  belongs to the yellow region defined in Eq. (6).

operators in Eq. (1) write explicitly as

$$\hat{K}_0 = \begin{pmatrix} 1 & 0 & 0 \\ 0 & \sqrt{1-\gamma_1} & 0 \\ 0 & 0 & \sqrt{1-\gamma_2-\gamma_3} \end{pmatrix}, \quad \hat{K}_{01} = \begin{pmatrix} 0 & \sqrt{\gamma_1} & 0 \\ 0 & 0 & 0 \\ 0 & 0 & 0 \end{pmatrix},$$

$$\hat{K}_{12} = \begin{pmatrix} 0 & 0 & 0 \\ 0 & 0 & \sqrt{\gamma_2} \\ 0 & 0 & 0 \end{pmatrix}, \quad \hat{K}_{03} = \begin{pmatrix} 0 & 0 & \sqrt{\gamma_3} \\ 0 & 0 & 0 \\ 0 & 0 & 0 \end{pmatrix}, \tag{5}$$

with CPTP conditions from Eq. (2) given by

$$\begin{cases} 0 \leq \gamma_j \leq 1, & \forall j = 1, 2, 3, \\ \gamma_2 + \gamma_3 \leq 1, \end{cases} \tag{6}$$

which produce the volume visualized in the bottom panel of Fig. 1.

The resulting mapping as in Eq. (3) for the channel  $\mathcal{D}_{(\gamma_1, \gamma_2, \gamma_3)}$  reduces, hence, to the following expression

$$\mathcal{D}_{\vec{\gamma}}(\hat{\rho}) = \begin{pmatrix} \rho_{00} + \gamma_1 \rho_{11} + \gamma_3 \rho_{22} & \sqrt{1-\gamma_1} \rho_{01} & \sqrt{1-\gamma_2-\gamma_3} \rho_{02} \\ \sqrt{1-\gamma_1} \rho_{01}^* & (1-\gamma_1) \rho_{11} + \gamma_2 \rho_{22} & \sqrt{1-\gamma_1} \sqrt{1-\gamma_2-\gamma_3} \rho_{12} \\ \sqrt{1-\gamma_2-\gamma_3} \rho_{02}^* & \sqrt{1-\gamma_1} \sqrt{1-\gamma_2-\gamma_3} \rho_{12}^* & (1-\gamma_2-\gamma_3) \rho_{22} \end{pmatrix}, \tag{7}$$

while the associated complementary CPTP transformation<sup>2,4-6</sup> computed as in Eq. (67) of “Methods”, for generic choices of the system parameters, transforms A into a four-dimensional state via the mapping

$$\hat{\mathcal{D}}_{\vec{\gamma}}(\hat{\rho}) = \begin{pmatrix} \rho_{00} + (1-\gamma_1)\rho_{11} + (1-\gamma_2-\gamma_3)\rho_{22} & \sqrt{\gamma_1}\rho_{01} & \sqrt{1-\gamma_1}\sqrt{\gamma_3}\rho_{12} & \sqrt{\gamma_3}\rho_{02} \\ \sqrt{\gamma_1}\rho_{01}^* & \gamma_1\rho_{11} & 0 & \sqrt{\gamma_1}\sqrt{\gamma_3}\rho_{12} \\ \sqrt{1-\gamma_1}\sqrt{\gamma_3}\rho_{12}^* & 0 & \gamma_2\rho_{22} & 0 \\ \sqrt{\gamma_3}\rho_{02}^* & \sqrt{\gamma_1}\sqrt{\gamma_3}\rho_{12}^* & 0 & \gamma_3\rho_{22} \end{pmatrix}, \tag{8}$$

where for  $i, j \in 0, 1, 2$ ,  $\rho_{ij} \equiv \langle i | \hat{\rho} | j \rangle$  are the matrix entries of the input density operator  $\hat{\rho} \in \mathfrak{S}(\mathcal{H}_A)$ .

**Quantum and private classical capacities for qutrit MAD.** The quantum capacity  $Q(\Phi)$  of a quantum channel  $\Phi$  is a measure of how faithfully quantum states can be transmitted from the input to the output of the associated CPTP map by exploiting proper encoding and decoding procedures that act on multiple transmission stages<sup>2,4-8</sup>. The private classical capacity  $C_p$  instead quantifies the amount of classical information transmittable per channel use under the extra requirement that the entire signaling process allows the communicating parties to be protected by eavesdropping by an adversary agent that is controlling the communication line. The explicit evaluation of these important functionals is one of the most elusive task of quantum information theory, as testified by the limited number of examples which allow for an explicit solution. A closed expression for the quantum capacity is provided by the formula<sup>44-46</sup>

$$Q(\Phi) = \lim_{n \rightarrow \infty} Q^{(n)}(\Phi)/n, \tag{9}$$

$$Q^{(n)}(\Phi) \equiv \max_{\hat{\rho}^{(n)} \in \mathfrak{S}(\mathcal{H}^{\otimes n})} J(\Phi^{\otimes n}, \hat{\rho}^{(n)}), \tag{10}$$

where the maximization in Eq. (10) is performed over the set of density matrices of  $n$  channel uses, and  $J$  is the coherent information

$$J(\Phi^{\otimes n}, \hat{\rho}^{(n)}) \equiv S(\Phi^{\otimes n}(\hat{\rho}^{(n)})) - S(\tilde{\Phi}^{\otimes n}(\hat{\rho}^{(n)})), \tag{11}$$

with  $S(\hat{\rho}) \equiv -\text{Tr}[\hat{\rho} \log_2 \hat{\rho}]$  the von Neumann entropy of the state  $\hat{\rho}$ , and  $\tilde{\Phi}$  the complementary channel of  $\Phi$ , see “Methods”—Complementary channels and degradability. For the private classical capacity instead, we have<sup>46,47</sup>:

$$C_p(\Phi) = \lim_{n \rightarrow \infty} C_p^{(n)}(\Phi)/n, \tag{12}$$

$$C_p^{(n)}(\Phi) \equiv \max_{\mathcal{E}_n} (\chi(\Phi^{\otimes n}, \mathcal{E}_n) - \chi(\tilde{\Phi}^{\otimes n}, \mathcal{E}_n)), \tag{13}$$

where the maximization is now performed over all quantum ensembles  $\mathcal{E}_n \equiv \{p_i, \hat{\rho}_i^{(n)}\}$  of  $n$  channel uses, and where

$$\chi(\Phi^{\otimes n}, \mathcal{E}_n) \equiv S\left(\Phi^{\otimes n}\left(\sum_i p_i \hat{\rho}_i^{(n)}\right)\right) - \sum_i p_i S\left(\Phi^{\otimes n}(\hat{\rho}_i^{(n)})\right) \tag{14}$$

is the Holevo information functional. The difficulties related to the evaluation of the above formulas are well known and ultimately the reason underlying our efforts here. An exception to this predicament is given by degradable<sup>48</sup> and antidegradable<sup>49</sup> channels. Degradable channels are those for which exists a CPTP map  $\mathcal{N}$  s.t.  $\tilde{\Phi} = \mathcal{N} \circ \Phi$ , while antidegradable channels are those for which exists a CPTP map  $\mathcal{M}$  s.t.  $\Phi = \mathcal{M} \circ \tilde{\Phi}$ ; for more details, see “Methods”—Complementary channels and degradability. For degradable channels,  $Q$  and  $C_p$  result to be additive, so the regularization over  $n$  in Eq. (9) is not needed, leading to the following single-letter formula<sup>50</sup>

$$C_p(\Phi) = Q(\Phi) = Q^{(1)}(\Phi). \tag{15}$$

For antidegradable channels instead, due to a no-cloning argument  $Q = 0$  while, from expression in Eq. (13), positivity of private classical capacities and data processing, we have  $C_p = 0$ . So no maximizations are needed.

Building up from these premises, here we present a thoughtful characterization of the quantum capacity  $Q(\mathcal{D}_{\vec{\gamma}})$  and the private classical capacity  $C_p(\mathcal{D}_{\vec{\gamma}})$  of the qutrit MAD channel  $\mathcal{D}_{\vec{\gamma}}$

defined in Eq. (7). We stress that while failing to provide the explicit solution for all rate vectors  $\vec{\gamma}$  in the allowed domain defined by Eq. (6), in what follows we manage to deliver the exact values of  $Q(\mathcal{D}_{\vec{\gamma}})$  and  $C_p(\mathcal{D}_{\vec{\gamma}})$  for a quite a large class of qutrit MAD channels by making use of degradability properties<sup>48</sup>, data-processing (or bottleneck) inequalities<sup>51,52</sup>, and channel isomorphism. In particular, we anticipate here that, for those  $\mathcal{D}_{\vec{\gamma}}$  which are provably degradable, we shall exploit the covariance property in Eq. (4) to further simplify the single-letter formula in Eq. (15) as

$$Q(\mathcal{D}_{\vec{\gamma}}) = C_p(\mathcal{D}_{\vec{\gamma}}) = \max_{\hat{\rho}_{\text{diag}}} \left\{ S(\mathcal{D}_{\vec{\gamma}}(\hat{\rho}_{\text{diag}})) - S(\tilde{\mathcal{D}}_{\vec{\gamma}}(\hat{\rho}_{\text{diag}})) \right\}, \quad (16)$$

where the maximization is performed on input states of A which are diagonal in the computational basis of the problem, i.e. the density matrices of the form  $\hat{\rho}_{\text{diag}} = \sum_{i=0}^2 p_i |i\rangle \langle i|$  with  $p_0, p_1, p_2 \in [0, 1]$  being usually called “populations” and fulfilling the normalization constraint  $p_0 + p_1 + p_2 = 1$ , see “Methods”, Eq. (82), and below for details. Notably, when applicable, Eq. (16) relies on an optimization of a functional of only  $d - 1$  real variables in the case of a qudit MAD and consequently just two real variables in the case of a qutrit MAD (namely the populations  $p_0$  and  $p_1$ ), which can be easily carried out (at least numerically).

To begin with, observe that, as anticipated in Eq. (8), the complementary map  $\tilde{\mathcal{D}}_{\vec{\gamma}}$  of a generic qutrit MAD channel  $\mathcal{D}_{\vec{\gamma}}$  sends the input states of A into a four-dimensional “environment state”. In the end, this is a consequence of the fact that the (minimal) number of Kraus operators we need to express Eq. (7) is 4. Unfortunately, this number also ensures us that the channel is not degradable: it has been indeed shown<sup>53</sup> that a necessary condition for any CPTP map with output dimension 3 to be degradable is that its associated Choi rank, and consequently the minimal number of Kraus operators we need to express such transformation, is at most 3. This brings us to consider some simplification in the problem, e.g. by fixing some of the values of the damping parameters. One approach is represented by the selective suppression of one (or two) of the decaying channels, i.e. imposing one (or two) of the parameters  $\gamma_i$  equal to 0 or to their maximum allowed value, choices that as we shall see, will effectively allow us to reduce the number of degrees of freedom of the problem.

*Single-decay qutrit MAD channels.* We consider here instances of the qutrit MAD channel in which only one of the three damping parameters  $\gamma_i$  is explicitly different from zero, i.e. the maps  $\mathcal{D}_{(\gamma_1, 0, 0)}$ ,  $\mathcal{D}_{(0, \gamma_2, 0)}$ , and  $\mathcal{D}_{(0, 0, \gamma_3)}$  associated, respectively, with the edges DA, DF, and DE of Fig. 1. It is easy to verify that these three sets of transformations can be mapped into each other via unitary conjugations that simply permute the energy levels of the system: for instance  $\mathcal{D}_{(0, 0, \gamma_3)}$  can be transformed into  $\mathcal{D}_{(\gamma_1, 0, 0)}$  by simply swapping levels |1⟩ and |2⟩. Accordingly, the capacities of these three sets must coincide, since each channel can be obtained from the other, i.e.

$$Q(\mathcal{D}_{(\gamma, 0, 0)}) = Q(\mathcal{D}_{(0, \gamma, 0)}) = Q(\mathcal{D}_{(0, 0, \gamma)}), \quad \forall \gamma \in [0, 1], \quad (17)$$

(similarly for  $C_p$ ). By virtue of this fact, without loss of generality, in the following we report the analysis only for  $\mathcal{D}_{(\gamma_1, 0, 0)}$ , being the results trivially extendable to the remaining two. For this purpose, we observe that from Eq. (5) it follows that  $\mathcal{D}_{(\gamma_1, 0, 0)}$  possesses only

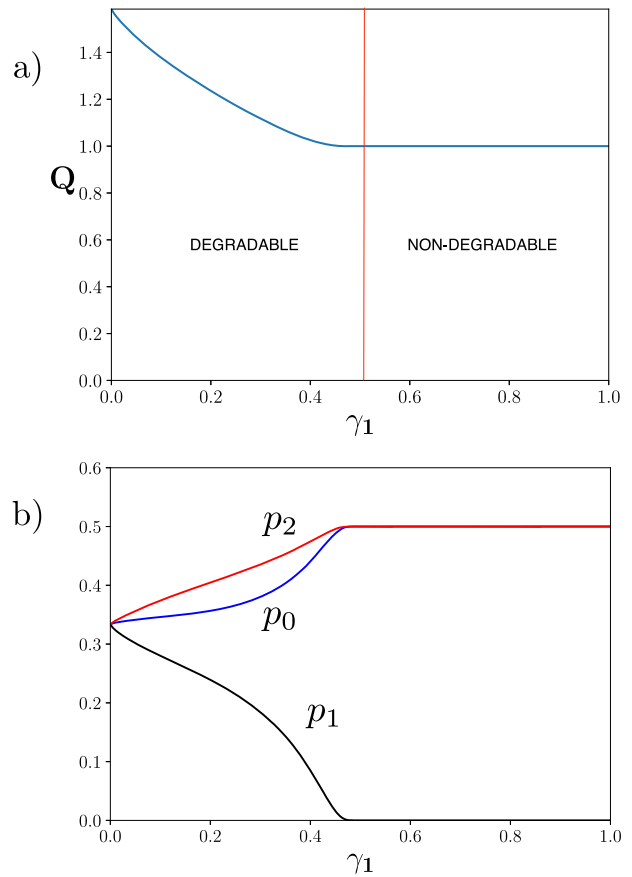


**Fig. 2 Quantum capacity for the single-decay.** **a** Profile of the quantum and the private classical capacity for the channel  $\mathcal{D}_{(\gamma_1, 0, 0)}$  w.r.t. the damping parameter  $\gamma_1$ . For  $\gamma_1 \leq 1/2$ , the channel is degradable and the reported value follows from the numerical maximization. For  $\gamma_1 > 1/2$ , instead, the channel is neither degradable nor antidegradable: here the associated capacity value is equal to 1. Notice that the reported values respect the monotonicity property given by Eq. (48). **b** Populations  $p_0$ ,  $p_1$ , and  $p_2$  of those states that maximize the quantum capacity formula for the channel  $\mathcal{D}_{(\gamma_1, 0, 0)}$  w.r.t. the damping parameter  $\gamma_1$ .

two non-zero Kraus operators, i.e.

$$\hat{K}_0 = \begin{pmatrix} 1 & 0 & 0 \\ 0 & \sqrt{1 - \gamma_1} & 0 \\ 0 & 0 & 1 \end{pmatrix} \quad \hat{K}_{01} = \begin{pmatrix} 0 & \sqrt{\gamma_1} & 0 \\ 0 & 0 & 0 \\ 0 & 0 & 0 \end{pmatrix}. \quad (18)$$

Transformation in Eq. (7) is then given by

$$\mathcal{D}_{(\gamma_1, 0, 0)}(\hat{\rho}) = \begin{pmatrix} \rho_{00} + \gamma_1 \rho_{11} & \sqrt{1 - \gamma_1} \rho_{01} & \rho_{02} \\ \sqrt{1 - \gamma_1} \rho_{01}^* & (1 - \gamma_1) \rho_{11} & \sqrt{1 - \gamma_1} \rho_{12} \\ \rho_{02}^* & \sqrt{1 - \gamma_1} \rho_{12}^* & \rho_{22} \end{pmatrix}, \quad (19)$$

and the complementary channel  $\tilde{\mathcal{D}}_{(\gamma_1, 0, 0)}$  that can be expressed as a mapping that connects the system A to a two-dimensional environmental system E, i.e.

$$\tilde{\mathcal{D}}_{(\gamma_1, 0, 0)}(\hat{\rho}) = \begin{pmatrix} 1 - \gamma_1 \rho_{11} & \sqrt{\gamma_1} \rho_{01} \\ \sqrt{\gamma_1} \rho_{01}^* & \gamma_1 \rho_{11} \end{pmatrix}. \quad (20)$$

By the study of degradability and the techniques discussed in “Methods” and in Supplementary Note 1, we are able to evaluate  $Q$  and  $C_p$  for every  $\gamma$ . The results are summarized in the plot in Fig. 2.

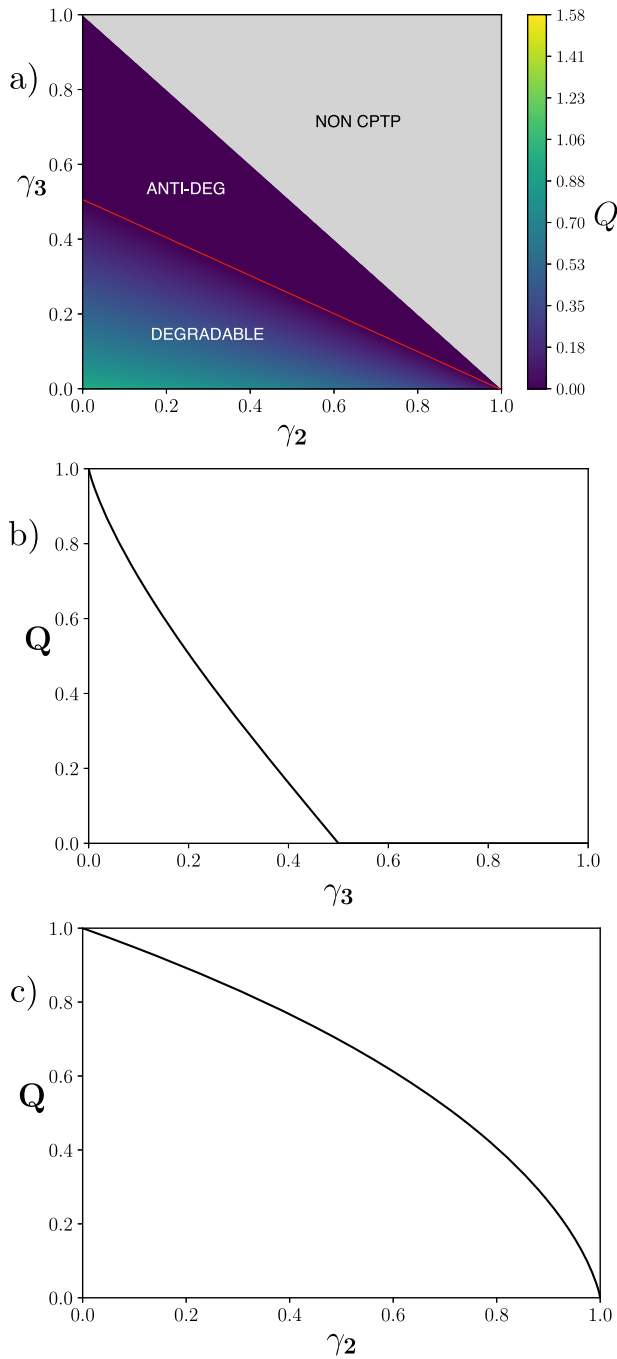


**Fig. 3** Quantum and private classical capacity of the channel  $\mathcal{D}_{(1,\gamma_2,\gamma_3)}$ . **a** Values for quantum ( $Q$ ) and private classical ( $C_p$ ) capacities (here they are identical) of the Multi-level Amplitude Damping channel  $\mathcal{D}_{(1,\gamma_2,\gamma_3)}$  w.r.t.  $\gamma_2$  and  $\gamma_3$ —the associated parameter region corresponds to the ABC triangle of Fig. 1. The gray region represent points where  $\mathcal{D}_{(1,\gamma_2,\gamma_3)}$  is not Completely Positive and Trace Preserving (CPTP); the points above the red line ( $\gamma_3 = (1 - \gamma_2)/2$ ) have zero capacity,  $Q(\mathcal{D}_{(1,\gamma_2,\gamma_3)}) = 0$ . For  $\gamma_2 = 0$ , the value of  $Q(\mathcal{D}_{(1,\gamma_2,\gamma_3)})$  and  $C_p(\mathcal{D}_{(1,\gamma_2,\gamma_3)})$  coincides with the quantum capacity of a qubit Amplitude Damping channel of transmissivity  $\gamma_3$  (ref. 9) (plot **b**): this should be compared with the value of  $Q(\mathcal{D}_{(1,\gamma_2,\gamma_3)})$  and the private classical capacity  $C_p(\mathcal{D}_{(1,\gamma_2,\gamma_3)})$  on the other border (i.e.  $\gamma_3 = 0$ ), which we report in **c**. Notice finally that the reported values respect the monotonicity requirement of Eq. (52).

Complete damping of the first excited state ( $\gamma_1 = 1$ ). Assume next that our qutrit MAD channel of Eq. (7) is characterized by the maximum value of  $\gamma_1$  allowed by CPTP constraint of Eq. (6), i.e.  $\gamma_1 = 1$ , region represented by the ABC triangle of Fig. 1. This map corresponds to the case where the initial population of the first excited level  $|1\rangle$  gets completely lost in favor of the ground state  $|0\rangle$  of the model so that Eqs. (7) and (8) rewrite as

$$\mathcal{D}_{(1,\gamma_2,\gamma_3)}(\hat{\rho}) = \begin{pmatrix} 1 - (1 - \gamma_3)\rho_{22} & 0 & \sqrt{1 - \gamma_2 - \gamma_3}\rho_{02} \\ 0 & \gamma_2\rho_{22} & 0 \\ \sqrt{1 - \gamma_2 - \gamma_3}\rho_{02}^* & 0 & (1 - \gamma_2 - \gamma_3)\rho_{22} \end{pmatrix}, \quad (21)$$

$$\tilde{\mathcal{D}}_{(1,\gamma_2,\gamma_3)}(\hat{\rho}) = \begin{pmatrix} \rho_{00} + (1 - \gamma_2 - \gamma_3)\rho_{22} & \rho_{01} & 0 & \sqrt{\gamma_3}\rho_{02} \\ \rho_{01}^* & \rho_{11} & 0 & \sqrt{\gamma_3}\rho_{12} \\ 0 & 0 & \gamma_2\rho_{22} & 0 \\ \sqrt{\gamma_3}\rho_{02}^* & \sqrt{\gamma_3}\rho_{12}^* & 0 & \gamma_3\rho_{22} \end{pmatrix}, \quad (22)$$

for  $\gamma_2, \gamma_3 \in [0, 1]$  such that  $\gamma_2 + \gamma_3 \leq 1$ . The above expressions make it explicit that, at variance with the case discussed in the previous section and in agreement with the conclusions of ref. 53, the map  $\mathcal{D}_{(1,\gamma_2,\gamma_3)}$  is not degradable. Indeed we notice that while  $\tilde{\mathcal{D}}_{(1,\gamma_2,\gamma_3)}(\hat{\rho})$  preserves information about the components  $\rho_{11}, \rho_{01}, \rho_{10}, \rho_{12}, \rho_{21}$  of the input state  $\hat{\rho}$ , no trace of those terms is left in  $\mathcal{D}_{(1,\gamma_2,\gamma_3)}(\hat{\rho})$ : accordingly it is technically impossible to identify a linear (not mentioning CPTP) map  $\mathcal{N}$  which applied to  $\mathcal{D}_{(1,\gamma_2,\gamma_3)}(\hat{\rho})$  would reproduce  $\tilde{\mathcal{D}}_{(1,\gamma_2,\gamma_3)}(\hat{\rho})$  for all  $\hat{\rho}$ . Despite this fact, it turns out that also for  $\mathcal{D}_{(1,\gamma_2,\gamma_3)}$ , the capacity can still be expressed as the single letter expression in Eq. (16). For the technical details, we refer the reader to Supplementary Note 2, where we apply techniques expressed in “Methods”. We report the results in Fig. 3.

Double-decay qutrit MAD channel with  $\gamma_2 = 0$ . Here we consider the value of the capacity for  $\vec{\gamma}$  belonging to the square surface ABED of Fig. 1, identified by the condition  $\gamma_2 = 0$ . From Eq. (5), we have that the Kraus operators for the MAD channel  $\mathcal{D}_{(\gamma_1,0,\gamma_3)}$  are three:

$$\hat{K}_0 = \begin{pmatrix} 1 & 0 & 0 \\ 0 & \sqrt{1 - \gamma_1} & 0 \\ 0 & 0 & \sqrt{1 - \gamma_3} \end{pmatrix}, \quad \hat{K}_{01} = \begin{pmatrix} 0 & \sqrt{\gamma_1} & 0 \\ 0 & 0 & 0 \\ 0 & 0 & 0 \end{pmatrix}, \quad (23)$$

$$\hat{K}_{03} = \begin{pmatrix} 0 & 0 & \sqrt{\gamma_3} \\ 0 & 0 & 0 \\ 0 & 0 & 0 \end{pmatrix}$$

while Eqs. (7) and (8) become

$$\mathcal{D}_{(\gamma_1,0,\gamma_3)}(\hat{\rho}) = \begin{pmatrix} \rho_{00} + \gamma_1\rho_{11} + \gamma_3\rho_{22} & \sqrt{1 - \gamma_1}\rho_{01} & \sqrt{1 - \gamma_3}\rho_{02} \\ \sqrt{1 - \gamma_1}\rho_{01}^* & (1 - \gamma_1)\rho_{11} & \sqrt{1 - \gamma_1}\sqrt{1 - \gamma_3}\rho_{12} \\ \sqrt{1 - \gamma_3}\rho_{02}^* & \sqrt{1 - \gamma_1}\sqrt{1 - \gamma_3}\rho_{12}^* & (1 - \gamma_3)\rho_{22} \end{pmatrix}, \quad (24)$$

$$\tilde{\mathcal{D}}_{(\gamma_1,0,\gamma_3)}(\hat{\rho}) = \begin{pmatrix} 1 - \gamma_1\rho_{11} - \gamma_3\rho_{22} & \sqrt{\gamma_1}\rho_{01} & \sqrt{\gamma_3}\rho_{02} \\ \sqrt{\gamma_1}\rho_{01}^* & \gamma_1\rho_{11} & \sqrt{\gamma_1}\sqrt{\gamma_3}\rho_{12} \\ \sqrt{\gamma_3}\rho_{02}^* & \sqrt{\gamma_1}\sqrt{\gamma_3}\rho_{12}^* & \gamma_3\rho_{22} \end{pmatrix}. \quad (25)$$

As evident from Fig. 2 and from the formal structure of Eq. (24), for  $\gamma_2 = 0$  the model exhibits a symmetry under the

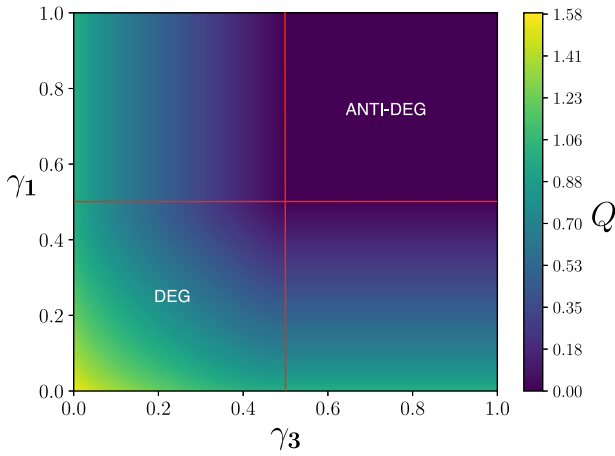


**Fig. 4 Quantum and private classical capacities of the channel  $\mathcal{D}_{(\gamma_1, 0, \gamma_3)}$ .** Quantum ( $Q$ ) and private classical ( $C_p$ ) capacities (here they coincide) for the channel  $\mathcal{D}_{(\gamma_1, 0, \gamma_3)}$  w.r.t. the damping parameters  $\gamma_1$  and  $\gamma_3$ . The damping parameters region  $(\gamma_1, 0, \gamma_3)$  coincides with the square surface ABED of Fig. 1. Notice that in the region  $\gamma_1, \gamma_3 \leq 1/2$  the channel is degradable as in Eq. (70), while for  $\gamma_1, \gamma_3 > 1/2$  the channel is antidegradable as in Eq. (71), in the remaining regions are neither degradable nor antidegradable.

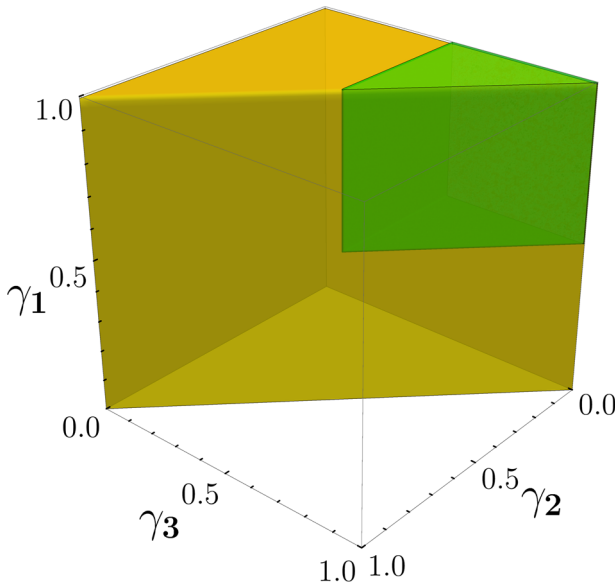


**Fig. 5 Parameter values corresponding to zero quantum capacity.** From antidegradability, Eq. (71), that implies that the quantum capacity  $Q = 0$ , bottleneck inequality that implies  $Q(\mathcal{M} \circ \mathcal{N}) \leq Q(\mathcal{N})$ ,  $Q(\mathcal{M})$  and composition rules, as shown in Supplementary Note 3, all points included in the green region of the plot have zero quantum (and private classical) capacity.

exchange of  $\gamma_1$  and  $\gamma_3$ . Indeed, indicating with  $\hat{V}$  the unitary gate that swaps levels  $|2\rangle$  and  $|3\rangle$  we have that

$$\mathcal{D}_{(\gamma_3, 0, \gamma_1)}(\hat{\rho}) = \hat{V} \mathcal{D}_{(\gamma_1, 0, \gamma_3)}(\hat{V} \hat{\rho} \hat{V}^\dagger) \hat{V}^\dagger, \quad (26)$$

which by data-processing inequality implies

$$Q(\mathcal{D}_{(\gamma_1, 0, \gamma_3)}) = Q(\mathcal{D}_{(\gamma_3, 0, \gamma_1)}), \quad (27)$$

with an analogous identity applying in the case of the private classical capacity. As reported in Supplementary Note 3, applying techniques in “Methods”, we produce results showed in Figs. 4 and 5.

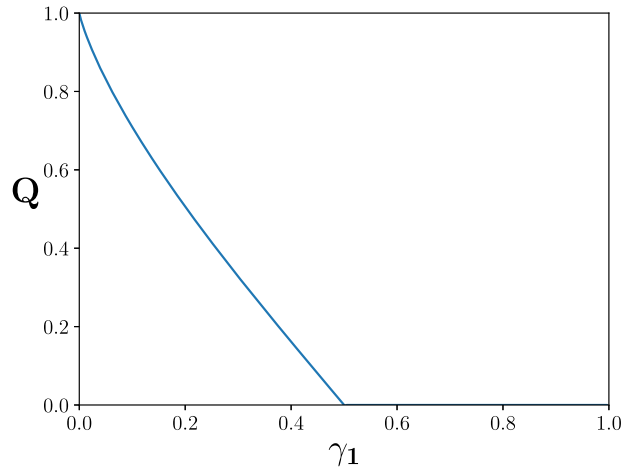


**Fig. 6 Quantum capacity of the channel  $\mathcal{D}_{(\gamma_1, \gamma_2, 1-\gamma_2)}$ .** Evaluation of the quantum capacity  $Q(\mathcal{D}_{(\gamma_1, \gamma_2, 1-\gamma_2)})$  w.r.t. the damping parameter  $\gamma_1$ , which is equal to the qubit ADC quantum capacity with damping parameter  $\gamma_1$  (ref. 9). The parameters region  $(\gamma_1, \gamma_2, 1-\gamma_2)$  corresponds to the rectangular region BEFC of Fig. 1: as shown in Eq. (31), the capacity exhibits no dependence upon the damping parameter  $\gamma_2$  in this case.

The qutrit MAD channel on the  $\gamma_2 + \gamma_3 = 1$  plane. Let us now consider the regime with  $\gamma_2 + \gamma_3 = 1$  where rate vectors  $\vec{\gamma}$  belong to the rectangular area BEFC of Fig. 1.

Under this condition, the map in Eq. (7) still admits four Kraus operators and becomes

$$\mathcal{D}_{(\gamma_1, \gamma_2, 1-\gamma_2)}(\hat{\rho}) = \begin{pmatrix} \rho_{00} + \gamma_1 \rho_{11} + (1-\gamma_2) \rho_{22} & \sqrt{1-\gamma_1} \rho_{01} & 0 \\ \sqrt{1-\gamma_1} \gamma_1 \rho_{01}^* & (1-\gamma_1) \rho_{11} + \gamma_2 \rho_{22} & 0 \\ 0 & 0 & 0 \end{pmatrix}. \quad (28)$$

We notice that the level  $|2\rangle$  gets completely depopulated and that the channel can be expressed as

$$\mathcal{D}_{(\gamma_1, \gamma_2, 1-\gamma_2)} = \mathcal{C} \circ \mathcal{D}_{\gamma_1}, \quad (29)$$

where  $\mathcal{D}_{\gamma_1}$  is a standard qubit ADC channel connecting level  $|1\rangle$  to level  $|0\rangle$  with damping rate  $\gamma_1$ , while now  $\mathcal{C}$  is a CPTP transformation sending the qutrit A to the qubit system spanned by vectors  $|0\rangle, |1\rangle$  and completely erasing the level  $|2\rangle$ , moving its population in part to  $|1\rangle$  and in part to  $|0\rangle$ , i.e.

$$\mathcal{C}(\hat{\rho}) = \begin{pmatrix} \rho_{00} + (1-\gamma_2) \rho_{22} & \rho_{01} \\ \rho_{10} & \rho_{11} + \gamma_2 \rho_{22} \end{pmatrix}. \quad (30)$$

Accordingly, the quantum capacity of  $\mathcal{D}_{\gamma_1}$  computed in ref. 9 is an explicit upper bound for  $Q(\mathcal{D}_{(\gamma_1, \gamma_2, 1-\gamma_2)})$  and  $C_p(\mathcal{D}_{(\gamma_1, \gamma_2, 1-\gamma_2)})$  (remember that for the qubit ADC  $Q$  and  $C_p$  coincide). On the other hand,  $Q(\mathcal{D}_{\gamma_1})$  is also a lower bound for  $Q(\mathcal{D}_{(\gamma_1, \gamma_2, 1-\gamma_2)})$  and  $C_p(\mathcal{D}_{(\gamma_1, \gamma_2, 1-\gamma_2)})$  as its rate can be achieved by simply using input states of A that live on the subspace  $\{|0\rangle, |1\rangle\}$ . Consequently, we can conclude that the following identity holds true

$$Q(\mathcal{D}_{(\gamma_1, \gamma_2, 1-\gamma_2)}) = C_p(\mathcal{D}_{(\gamma_1, \gamma_2, 1-\gamma_2)}) = Q(\mathcal{D}_{\gamma_1}), \quad (31)$$

as shown in Fig. 6.

Double-decay qutrit MAD channel with  $\gamma_1 = 0$ . Here we consider the triangular surface DEF of Fig. 1. From Eq. (1), we have that

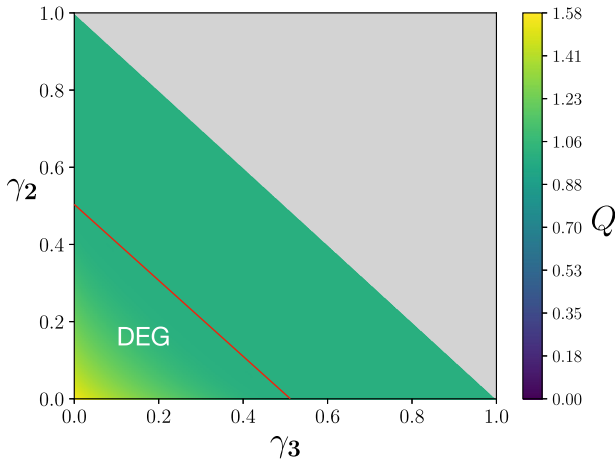


**Fig. 7 Quantum and private classical capacity of the channel  $\mathcal{D}_{(0, \gamma_2, \gamma_3)}$ .** Evaluation of the quantum ( $Q$ ) and private classical ( $C_p$ ) capacities, here they coincide, for  $\mathcal{D}_{(0, \gamma_2, \gamma_3)}$  w.r.t. the damping parameters  $\gamma_2$  and  $\gamma_3$ . The parameters region  $(0, \gamma_2, \gamma_3)$  corresponds to the triangular surface DEF of Fig. 1. The DEG (degradable) zone below the red curve,  $\gamma_2 + \gamma_3 = \frac{1}{2}$ , is the degradability region for the channel: here we compute  $Q(\mathcal{D}_{(0, \gamma_2, \gamma_3)})$  solving numerically the maximization of Supplementary Eq. (40). Above the red curve, the channel capacity assumes constant value from Eq. (36). Notice that the quantum capacity exhibits the symmetry as in Eq. (35) and the monotonicity conditions from Eq. (52). The gray zone indicates the non-accessible region, since it violates constraints in Eq. (6).

the Kraus operators for the MAD channel  $\mathcal{D}_{(0, \gamma_2, \gamma_3)}$  are three:

$$\hat{K}_0 = \begin{pmatrix} 1 & 0 & 0 \\ 0 & 0 & 0 \\ 0 & 0 & \sqrt{1 - \gamma_2 - \gamma_3} \end{pmatrix}, \quad \hat{K}_{12} = \begin{pmatrix} 0 & 0 & 0 \\ 0 & 0 & \sqrt{\gamma_2} \\ 0 & 0 & 0 \end{pmatrix},$$

$$\hat{K}_{03} = \begin{pmatrix} 0 & 0 & \sqrt{\gamma_3} \\ 0 & 0 & 0 \\ 0 & 0 & 0 \end{pmatrix}. \tag{32}$$

The actions of  $\mathcal{D}_{(0, \gamma_2, \gamma_3)}$  and its complementary counterpart  $\tilde{\mathcal{D}}_{(0, \gamma_2, \gamma_3)}$  on a generic density matrix  $\hat{\rho}$  can hence be described as

$$\mathcal{D}_{(0, \gamma_2, \gamma_3)}(\hat{\rho}) = \begin{pmatrix} \rho_{00} + \gamma_3 \rho_{22} & \rho_{01} & \sqrt{1 - \gamma_2 - \gamma_3} \rho_{02} \\ \rho_{01}^* & \rho_{11} + \gamma_2 \rho_{22} & \sqrt{1 - \gamma_2 - \gamma_3} \rho_{12} \\ \sqrt{1 - \gamma_2 - \gamma_3} \rho_{02}^* & \sqrt{1 - \gamma_2 - \gamma_3} \rho_{12}^* & (1 - \gamma_2 - \gamma_3) \rho_{22} \end{pmatrix}, \tag{33}$$

$$\tilde{\mathcal{D}}_{(0, \gamma_2, \gamma_3)}(\hat{\rho}) = \begin{pmatrix} 1 - (\gamma_2 + \gamma_3) \rho_{22} & \sqrt{\gamma_2} \rho_{12} & \sqrt{\gamma_3} \rho_{02} \\ \sqrt{\gamma_2} \rho_{12}^* & \gamma_2 \rho_{22} & 0 \\ \sqrt{\gamma_3} \rho_{02}^* & 0 & \gamma_3 \rho_{22} \end{pmatrix}, \tag{34}$$

(notice that in this case, differently of what happens with  $\mathcal{D}_{(\gamma_1, 0, \gamma_3)}$ , the complementary channel is not an element of the MAD set). By close inspection of Eq. (33), and as intuitively suggested by Fig. 1, also these channels exhibit a symmetry analogous to the one reported in Eq. (26), but this time with  $\hat{V}$  being the swap operation exchanging levels  $|0\rangle$  and  $|1\rangle$ , which gives us

$$Q(\mathcal{D}_{(0, \gamma_2, \gamma_3)}) = Q(\mathcal{D}_{(0, \gamma_3, \gamma_2)}), \tag{35}$$

and an analogous identity for the private classical capacity. Furthermore, as in the case of the single-decay qutrit MAD channel  $\mathcal{D}_{(0, \gamma_2, 0)}$ , we notice that  $\mathcal{D}_{(0, \gamma_2, \gamma_3)}$  has a noiseless subspace,

given here by  $\{|0\rangle, |1\rangle\}$ , and we can establish the following lower bound:

$$C_p(\mathcal{D}_{(0, \gamma_2, \gamma_3)}) \geq Q(\mathcal{D}_{(0, \gamma_2, \gamma_3)}) \geq \log_2(2) = 1. \tag{36}$$

In particular, this tells us that  $\mathcal{D}_{(0, \gamma_2, \gamma_3)}$  cannot be antidegradable (the same conclusion can be obtained by noticing that<sup>53</sup> the map  $\tilde{\mathcal{D}}_{(\gamma_2, 0, \gamma_3)}$  has a kernel that cannot be included into the kernel set of  $\mathcal{D}_{(\gamma_2, 0, \gamma_3)}$ —e.g. the former contains  $|0\rangle\langle 1|$  while the latter does not).

Following the usual approach—see Supplementary Note 4—we find that  $\mathcal{D}_{(0, \gamma_2, \gamma_3)}$  is invertible for  $\gamma_2 + \gamma_3 < 1$ , and that  $\tilde{\mathcal{D}}_{(0, \gamma_2, \gamma_3)} \circ \mathcal{D}_{(0, \gamma_2, \gamma_3)}^{-1}$  is CPTP for  $\gamma_2 + \gamma_3 \leq \frac{1}{2}$ , which defines hence the degradability region for the map. So, invoking Eq. (16) and the procedures described in “Methods”, we compute there the quantum capacity.

Via numerical inspection, we are also able to evaluate the magnitude of  $Q$  on the border of the degradability region, designated by  $\gamma_2 + \gamma_3 = \frac{1}{2}$ , showing that here it equals the lower bound in Eq. (36). This, in addition to the monotonicity in Eq. (52), allows us to conclude that  $Q$  assumes the value 1 over all the region above the degradability borderline (red curve of Fig. 7), i.e.

$$Q(\mathcal{D}_{(0, \gamma_2, \gamma_3)}) = C_p(\mathcal{D}_{(0, \gamma_2, \gamma_3)}) = 1, \quad \forall \gamma_2 + \gamma_3 \geq 1/2. \tag{37}$$

*Double-decay qutrit MAD channel with  $\gamma_3 = 0$ .* Here we consider the square region CADF of Fig. 1 identified by  $\gamma_3 = 0$ . From Eq. (1), we have that the Kraus operators for  $\mathcal{D}_{(\gamma_1, \gamma_2, 0)}$  are three:

$$\hat{K}_0 = \begin{pmatrix} 1 & 0 & 0 \\ 0 & \sqrt{1 - \gamma_1} & 0 \\ 0 & 0 & \sqrt{1 - \gamma_2} \end{pmatrix}, \quad \hat{K}_{01} = \begin{pmatrix} 0 & \sqrt{\gamma_1} & 0 \\ 0 & 0 & 0 \\ 0 & 0 & 0 \end{pmatrix},$$

$$\hat{K}_{02} = \begin{pmatrix} 0 & 0 & 0 \\ 0 & 0 & \sqrt{\gamma_2} \\ 0 & 0 & 0 \end{pmatrix}, \tag{38}$$

while the actions of  $\mathcal{D}_{(\gamma_1, \gamma_2, 0)}$  and  $\tilde{\mathcal{D}}_{(\gamma_1, \gamma_2, 0)}$  on a generic density matrix  $\hat{\rho}$  are:

$$\mathcal{D}_{(\gamma_1, \gamma_2, 0)}(\hat{\rho}) = \begin{pmatrix} \rho_{00} + \gamma_1 \rho_{11} & \sqrt{1 - \gamma_1} \rho_{01} & \sqrt{1 - \gamma_2} \rho_{02} \\ \sqrt{1 - \gamma_1} \rho_{01}^* & (1 - \gamma_1) \rho_{11} + \gamma_2 \rho_{22} & \sqrt{1 - \gamma_1} \sqrt{1 - \gamma_2} \rho_{12} \\ \sqrt{1 - \gamma_2} \rho_{02}^* & \sqrt{1 - \gamma_1} \sqrt{1 - \gamma_2} \rho_{12}^* & (1 - \gamma_2) \rho_{22} \end{pmatrix}, \tag{39}$$

$$\tilde{\mathcal{D}}_{(\gamma_1, \gamma_2, 0)}(\hat{\rho}) = \begin{pmatrix} 1 - \gamma_1 \rho_{11} - \gamma_2 \rho_{22} & \sqrt{\gamma_1} \rho_{01} & \sqrt{1 - \gamma_1} \sqrt{\gamma_2} \rho_{02} \\ \sqrt{\gamma_1} \rho_{01}^* & \gamma_1 \rho_{11} & 0 \\ \sqrt{1 - \gamma_1} \sqrt{\gamma_2} \rho_{02}^* & 0 & \gamma_2 \rho_{22} \end{pmatrix}. \tag{40}$$

At variance with the previous sections, we have that while  $\mathcal{D}_{(\gamma_1, \gamma_2, 0)}$  is invertible for  $\gamma_1, \gamma_2 < 1$ , for no range of these values the application  $\tilde{\mathcal{D}}_{(\gamma_1, \gamma_2, 0)} \circ \mathcal{D}_{(\gamma_1, \gamma_2, 0)}^{-1}$  produces a CPTP map. We can hence conclude that the map is never degradable. About antidegradability, here also we have that  $\ker\{\tilde{\mathcal{D}}_{(\gamma_1, \gamma_2, 0)}\} \not\subseteq \ker\{\mathcal{D}_{(\gamma_1, \gamma_2, 0)}\}$ , so  $\mathcal{D}_{(\gamma_1, \gamma_2, 0)}$  is also not antidegradable<sup>53</sup>. As a matter of fact, the only cases for which we can produce explicit values of  $Q(\mathcal{D}_{(\gamma_1, \gamma_2, 0)})$  are the limiting cases where either  $\gamma_1$  or  $\gamma_2$  equals 0 (in these cases, the map is a single-rate MAD channel discussed in “Results”—(Single-decay qutrit MAD channels), or 1 where instead findings of

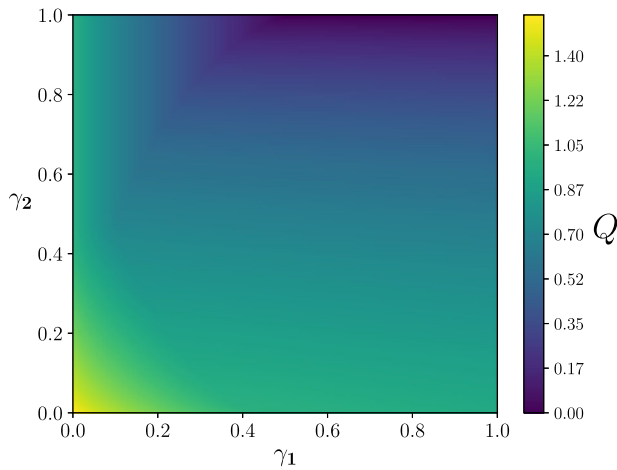


**Fig. 8 Lower bound for the quantum and private classical capacities of the channel  $\mathcal{D}_{(\gamma_1, \gamma_2, 0)}$ .** Numerical evaluation of a lower bound for the quantum capacity  $Q$  and the private classical capacity  $C_p$ , here they coincide, w.r.t. the damping parameters  $\gamma_1, \gamma_2$ . It is obtained by maximizing the single-use coherent information of the channel over all possible diagonal inputs. The parameters region  $(\gamma_1, \gamma_2, 0)$  corresponds to the CADF square of Fig. 1. Notice that reported plot does not fulfill the monotonicity constraint in Eq. (52), hence explicitly proving that the function we present is certainly not the real capacity of the system.

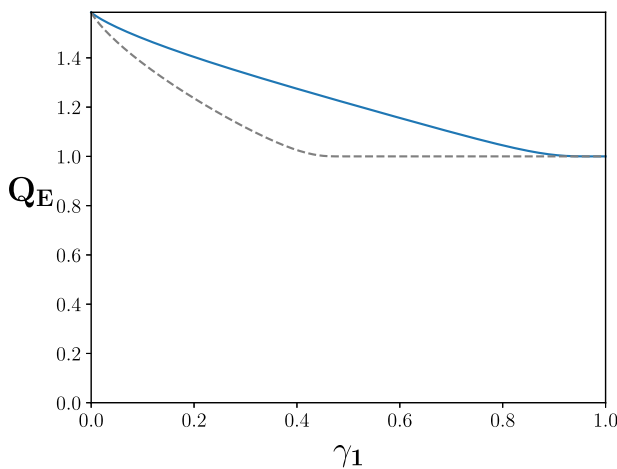


**Fig. 9 Entanglement-assisted quantum capacity for the single-decay channel.** Profile of the entanglement-assisted quantum capacity  $Q_E$  (blue) of the channel  $\mathcal{D}_{(\gamma_1, 0, 0)}$  w.r.t. the damping parameter  $\gamma_1$  (results should be compared with those of Fig. 2 where we present the quantum capacity  $Q(\mathcal{D}_{(\gamma_1, 0, 0)})$  (dashed gray)). Notice that also in this case the expression fulfills the monotonicity constraint in Eq. (48).

“Results”—(Complete damping of the first excited state ( $\gamma_1 = 1$ )) or Results—(The qutrit MAD channel on the  $\gamma_2 + \gamma_3 = 1$  plane) can be applied. For the remaining cases, we resort in presenting a lower bound for  $Q(\mathcal{D}_{(\gamma_1, \gamma_2, 0)})$  and  $C_p(\mathcal{D}_{(\gamma_1, \gamma_2, 0)})$ .

A straightforward approach is to exploit the right-hand-side of Eq. (16) and run them also outside the degradability region, in synthesis evaluating the maximum of the coherent information of  $\mathcal{D}_{(\gamma_1, \gamma_2, 0)}$  on the diagonal sources. Notice that since the map is not degradable, the coherent information is not necessarily concave and the restriction to diagonal sources does not even guarantee that the computed expression corresponds to the true

$Q^{(1)}(\mathcal{D}_{(\gamma_1, \gamma_2, 0)})$  functional. Clearly the task can be refined as much as needed, e.g. by choosing less specific families of states or by computing  $Q^{(i)}(\mathcal{D}_{(\gamma_1, \gamma_2, 0)})$  for  $i > 1$ , but these aspects are beyond the focus of this work and will be considered in future research. The results we obtain are reported in Fig. 8.

**Entanglement-assisted quantum capacity of qutrit MAD channels.** For the sake of completeness, the present section is devoted to studying the entanglement-assisted quantum capacity  $Q_E(\mathcal{D})$  of MAD CPTP maps which quantifies the amount of quantum information transmittable per channel use assuming the communicating parties to share an arbitrary amount of entanglement. A closed expression for it has been provided in ref. 54,55 and results in an expression which, in contrast to the quantum capacity formula, does not need a regularization w.r.t. to the number of channel uses, i.e.

$$Q_E(\Phi) = \frac{1}{2} \max_{\hat{\rho} \in \mathfrak{E}(\mathcal{H})} I(\Phi, \hat{\rho}), \tag{41}$$

where now

$$\begin{aligned} I(\Phi, \hat{\rho}) &\equiv S(\hat{\rho}) + J(\Phi, \hat{\rho}) \\ &= S(\hat{\rho}) + S(\Phi(\hat{\rho})) - S(\tilde{\Phi}(\hat{\rho})), \end{aligned} \tag{42}$$

is the quantum mutual information functional. The discussion in “Methods” about covariance of the channel and the concavity—in this case of the quantum mutual information—apply also here, and we can reduce the maximization in Eq. (41) to

$$Q_E(\mathcal{D}) = \frac{1}{2} \max_{\hat{\rho}_{\text{diag}}} \left\{ S(\hat{\rho}_{\text{diag}}) + S(\mathcal{D}(\hat{\rho}_{\text{diag}})) - S(\tilde{\mathcal{D}}(\hat{\rho}_{\text{diag}})) \right\}, \tag{43}$$

where  $\hat{\rho}_{\text{diag}}$  are input density matrices which are diagonal in the computational basis of the system, see Supplementary Note 5. The evaluations of  $Q_E$  of the for the single and double-decay qutrit MAD channels are reported in Figs. 9 and 10. Notice that also the three-rate qutrit MAD channels  $Q_E$  can be computed but not easily visualized, hence it is not reported.

**Conclusion.** We introduce a finite dimensional generalization of the qubit ADC model which represents one of the most studied examples of quantum noise in quantum information theory. In this context, the quantum (and classical private) capacity of a large class of quantum channels (namely the qutrit MAD channels) has been explicitly computed, vastly extending the set of models whose capacity is known: this effort in particular includes some non-trivial examples of quantum maps which are explicitly non-degradable (neither antidegradable)—see e.g. the results of “Methods”—(Double-decay qutrit MAD channel with  $\gamma_3 = 0$ ). Having also shown the covariance w.r.t. diagonalizing unitaries of the MAD, follows that, when degradable, the computational complexity associated with the quantum capacity evaluation grows only linearly with the dimension. Besides allowing generalizations to higher dimensional systems (see e.g. ref. 33), the analysis here presented naturally spawns further research, e.g. extending it to include other capacity measures, such as the classical capacity or the two-way quantum capacity<sup>52,56</sup>. We finally conclude by noticing that the MAD channel scheme discussed in the present paper can be also easily adapted to include generalizations of the (qubit) generalized ADC scheme<sup>52</sup>, by allowing reverse damping processes which promote excitations from lower to higher levels that could mimic, e.g., thermalization events.



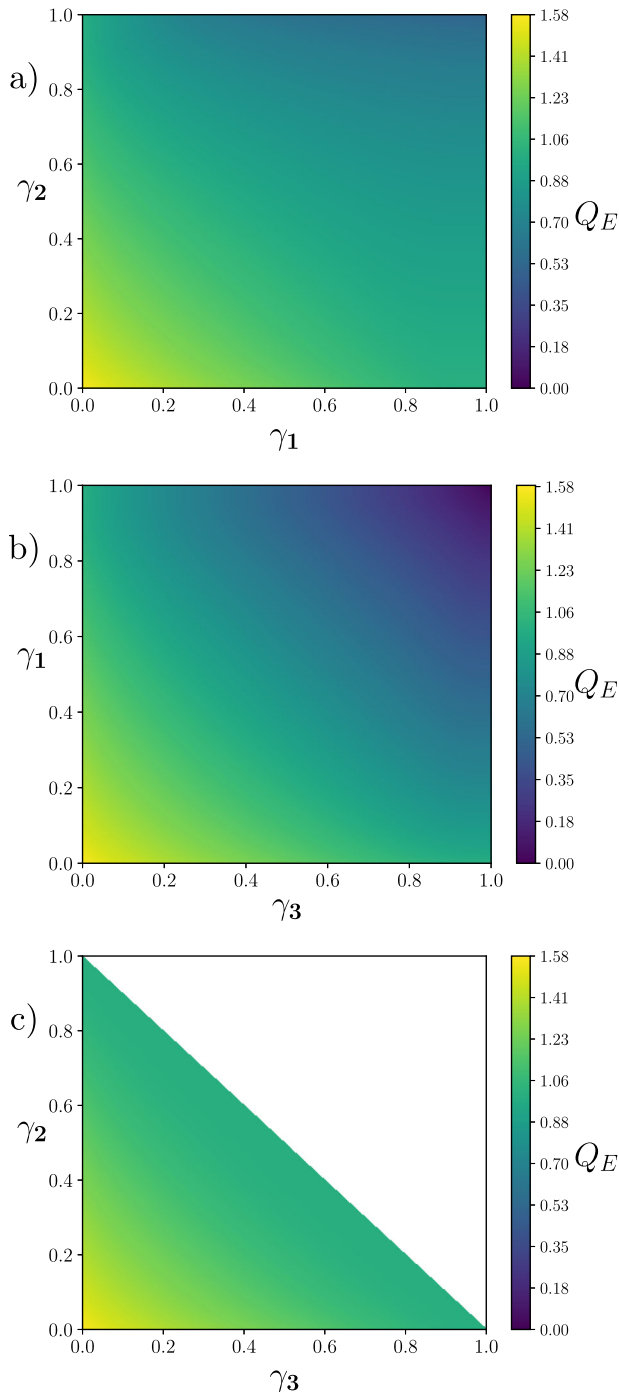


**Fig. 10 Entanglement-assisted quantum capacity for double-decay channels.** **a** Entanglement-assisted quantum capacity  $Q_E$  of the channel  $\mathcal{D}_{(\gamma_1, \gamma_2, 0)}$  w.r.t. the damping parameter  $\gamma_1, \gamma_2$ , the parameters region  $(\gamma_1, \gamma_2, 0)$  corresponds to the CADF square region of Fig. 1. **b** Entanglement-assisted quantum capacity  $Q_E$  of the channel  $\mathcal{D}_{(\gamma_1, 0, \gamma_3)}$  w.r.t. the damping parameter  $\gamma_1, \gamma_3$ , the parameters region  $(\gamma_1, 0, \gamma_3)$  corresponds to the ABED region of Fig. 1. **c** Entanglement-assisted quantum capacity  $Q_E$  of the channel  $\mathcal{D}_{(0, \gamma_2, \gamma_3)}$  w.r.t. the damping parameter  $\gamma_2, \gamma_3$ , the parameters region  $(0, \gamma_2, \gamma_3)$  corresponds to the DEF region of Fig. 1.

**Methods**

**Composition rules, data-processing, bottleneck inequalities.** It is relatively easy to verify that the set of qutrit MAD channels in Eq. (7) is closed under concatenation. Specifically we notice that given  $\mathcal{D}_{\vec{\gamma}}$  and  $\mathcal{D}_{\vec{\gamma}'}$  with  $\vec{\gamma}' = (\gamma'_1, \gamma'_2, \gamma'_3)$

and  $\vec{\gamma} = (\gamma_1, \gamma_2, \gamma_3)$  two rate vectors fulfilling the conditions in Eq. (6), we have

$$\mathcal{D}_{\vec{\gamma}} \circ \mathcal{D}_{\vec{\gamma}'} = \mathcal{D}_{\vec{\gamma}}, \tag{44}$$

with  $\vec{\gamma} = (\gamma_1, \gamma_2, \gamma_3)$  a new rate vector of components

$$\begin{cases} \gamma_1 = \gamma'_1 + \gamma'_1 - \gamma'_1 \gamma'_1, \\ \gamma_2 = \gamma'_2(1 - \gamma'_1 - \gamma'_2) + \gamma'_2(1 - \gamma'_3), \\ \gamma_3 = \gamma'_3 + \gamma'_2(\gamma'_1 - \gamma'_3) + \gamma'_3(1 - \gamma'_3). \end{cases} \tag{45}$$

which also satisfies Eq. (6). The importance of Eq. (44) for the problem we are facing stems from channel data-processing inequalities (or bottleneck inequalities)<sup>7,51,52</sup>, according to which, any information capacity functional  $\Gamma$  (ref. 2) such as the quantum capacity  $Q$ , the classical capacity  $C$ , the private classical capacity  $C_p$ , the entanglement-assisted classical capacity  $C_E$  etc., computed for a CPTP map  $\Phi = \Phi' \circ \Phi''$  obtained by concatenating channel  $\Phi'$  with channel  $\Phi''$ , must fulfill the following relation

$$\Gamma(\Phi) \leq \min\{\Gamma(\Phi'), \Gamma(\Phi'')\}. \tag{46}$$

Applied to Eq. (44), the above inequality can be used to predict monotonic behaviors for the capacity  $\Gamma(\mathcal{D}_{\vec{\gamma}})$  as a function of the rate vector  $\vec{\gamma}$ , that allows us to provide useful lower and upper bounds which in some case permit to extend the capacity formula to domain where other techniques (e.g. degradability analysis) fail. In particular, we notice that for single-decay MAD channels where only one component of the rate vector is different from zero (say  $\gamma_1$ ), we get

$$\mathcal{D}_{(\gamma_1, 0, 0)} \circ \mathcal{D}_{(\gamma'_1, 0, 0)} = \mathcal{D}_{(\gamma'_1, 0, 0)} \circ \mathcal{D}_{(\gamma_1, 0, 0)} = \mathcal{D}_{(\gamma_1, 0, 0)}, \tag{47}$$

with  $\gamma_1$  as in the first identity of Eq. (45). Accordingly, we can conclude that all the capacities  $\Gamma(\mathcal{D}_{(\gamma_1, 0, 0)})$  should be non-increasing functionals of the parameter  $\gamma_1$ , i.e.

$$\Gamma(\mathcal{D}_{(\gamma_1, 0, 0)}) \geq \Gamma(\mathcal{D}_{(\gamma', 0, 0)}), \quad \forall \gamma_1 \leq \gamma', \tag{48}$$

(the same expressions and conclusions apply also for  $\mathcal{D}_{(0, \gamma_2, 0)}$  and  $\mathcal{D}_{(0, 0, \gamma_3)}$ ). Composing two single-decay MAD channels characterized by rate vectors pointing along different cartesian axis in general can create maps with a resulting vector rate with a component in the third direction. Specifically from Eq. (44) it follows that, for an arbitrary choice of the rate vector  $\vec{\gamma}' = (\gamma'_1, \gamma'_2, \gamma'_3)$  in the allowed CPTP domain, the MAD channel  $\mathcal{D}_{(\gamma_1, \gamma_2, \gamma_3)}$  can be expressed as

$$\mathcal{D}_{(\gamma_1, \gamma_2, \gamma_3)} = \mathcal{D}_{(0, 0, \gamma_3)} \circ \mathcal{D}_{(0, \gamma_2, 0)} \circ \mathcal{D}_{(\gamma_1, 0, 0)} \tag{49}$$

$$= \mathcal{D}_{(0, \bar{\gamma}_2, 0)} \circ \mathcal{D}_{(0, 0, \bar{\gamma}_3)} \circ \mathcal{D}_{(\gamma_1, 0, 0)}, \tag{50}$$

with

$$\bar{\gamma}_3 \equiv \frac{\gamma_3}{1 - \gamma_2}, \quad \bar{\gamma}_2 \equiv \frac{\gamma_2}{1 - \gamma_3}, \tag{51}$$

which because of the constraint in Eq. (6) are properly defined rates. As a direct consequence of Eqs. (46) and (47), it then follows that the capacities  $\Gamma(\mathcal{D}_{(\gamma_1, \gamma_2, \gamma_3)})$  must be non-increasing functionals of all the cartesian components of rate vector  $\vec{\gamma}$ , i.e.

$$\Gamma(\mathcal{D}_{(\gamma_1, \gamma_2, \gamma_3)}) \geq \Gamma(\mathcal{D}_{(\gamma'_1, \gamma'_2, \gamma'_3)}), \quad \forall \gamma'_i \geq \gamma_i, \tag{52}$$

and must be restricted by the upper bound

$$\Gamma(\mathcal{D}_{(\gamma_1, \gamma_2, \gamma_3)}) \leq \min\left\{\Gamma(\mathcal{D}_{(\gamma_1, 0, 0)}), \mathcal{D}_{(0, \bar{\gamma}_2, 0)}, \mathcal{D}_{(0, 0, \bar{\gamma}_3)}\right\}. \tag{53}$$

As a further refinement notice that, setting  $\gamma_2 = 0$  in Eqs. (49) and (50), we get

$$\mathcal{D}_{(\gamma_1, 0, \gamma_3)} = \mathcal{D}_{(\gamma_1, 0, 0)} \circ \mathcal{D}_{(0, 0, \gamma_3)} = \mathcal{D}_{(0, 0, \gamma_3)} \circ \mathcal{D}_{(\gamma_1, 0, 0)}, \tag{54}$$

which replaced back into Eq. (50) gives us

$$\mathcal{D}_{(\gamma_1, \gamma_2, \gamma_3)} = \mathcal{D}_{(0, \bar{\gamma}_2, 0)} \circ \mathcal{D}_{(\gamma_1, 0, \gamma_3)}, \tag{55}$$

which allows us to replace Eq. (53) with the stronger requirement

$$\Gamma(\mathcal{D}_{(\gamma_1, \gamma_2, \gamma_3)}) \leq \min\left\{\Gamma(\mathcal{D}_{(0, \bar{\gamma}_2, 0)}), \Gamma(\mathcal{D}_{(\gamma_1, 0, \gamma_3)})\right\}. \tag{56}$$

Similarly by setting  $\gamma_1 = 0$ , we get

$$\mathcal{D}_{(0, \gamma_2, \gamma_3)} = \mathcal{D}_{(0, 0, \bar{\gamma}_3)} \circ \mathcal{D}_{(0, \gamma_2, 0)} = \mathcal{D}_{(0, \bar{\gamma}_2, 0)} \circ \mathcal{D}_{(0, 0, \bar{\gamma}_3)}, \tag{57}$$

that yields

$$\mathcal{D}_{(\gamma_1, \gamma_2, \gamma_3)} = \mathcal{D}_{(0, \gamma_2, \gamma_3)} \circ \mathcal{D}_{(\gamma_1, 0, 0)}, \tag{58}$$

and

$$\Gamma(\mathcal{D}_{(\gamma_1, \gamma_2, \gamma_3)}) \leq \min\left\{\Gamma(\mathcal{D}_{(0, \gamma_2, \gamma_3)}), \Gamma(\mathcal{D}_{(\gamma_1, 0, 0)})\right\}. \tag{59}$$

Finally setting  $\gamma_3 = 0$  in Eq. (49), we get

$$\mathcal{D}_{(\gamma_1, \gamma_2, 0)} = \mathcal{D}_{(0, \gamma_2, 0)} \circ \mathcal{D}_{(\gamma_1, 0, 0)}, \tag{60}$$

that leads to

$$\mathcal{D}_{(\gamma_1, \gamma_2, \gamma_3)} = \mathcal{D}_{(0,0,\bar{\gamma}_3)} \circ \mathcal{D}_{(\gamma_1, \gamma_2, 0)}, \quad (61)$$

and

$$\Gamma(\mathcal{D}_{(\gamma_1, \gamma_2, \gamma_3)}) \leq \min\{\Gamma(\mathcal{D}_{(\gamma_1, \gamma_2, 0)}), \mathcal{D}_{(0,0,\bar{\gamma}_3)}\}. \quad (62)$$

**Complementary channels and degradability.** A CPTP map  $\Phi : \mathcal{L}(\mathcal{H}_A) \rightarrow \mathcal{L}(\mathcal{H}_B)$  can be seen as the evolution induced by an isometry  $\hat{V} : \mathcal{H}_A \rightarrow \mathcal{H}_B \otimes \mathcal{H}_E$  involving an environment  $E$ , called Stinespring dilation<sup>57,58</sup>. Specifically for all input states  $\rho_A \in \mathfrak{E}_A$  we can write

$$\Phi(\hat{\rho}_A) = \text{Tr}_E[\hat{V}\hat{\rho}_A\hat{V}^\dagger]. \quad (63)$$

If instead we trace out the degrees of freedom in  $B$ , we obtain the complementary (or conjugate) channel  $\tilde{\Phi} : \mathcal{L}(\mathcal{H}_A) \rightarrow \mathcal{L}(\mathcal{H}_E)$ , i.e.

$$\tilde{\Phi}(\hat{\rho}_A) = \text{Tr}_B[\hat{V}\hat{\rho}_A\hat{V}^\dagger]. \quad (64)$$

Being  $\hat{M}_k$  the Kraus operators generating  $\Phi$  and  $|k\rangle_E$  a basis for the environment, the operator  $\hat{V}$  can be written as:

$$\hat{V} = \sum_k \hat{M}_k \otimes |k\rangle_E, \quad (65)$$

and being

$$\hat{V}\hat{\rho}_A\hat{V}^\dagger = \sum_{ij} \hat{M}_i \hat{\rho}_A \hat{M}_j^\dagger \otimes |i\rangle\langle j|_E, \quad (66)$$

it is straightforward to verify that Eq. (64) can be equivalently expressed as

$$\tilde{\Phi}(\hat{\rho}_A) = \sum_{ij} \text{Tr}_B[\hat{M}_i \hat{\rho}_A \hat{M}_j^\dagger] |i\rangle\langle j|_E. \quad (67)$$

A fact that it is worth mentioning, as it will play a fundamental role in our analysis, is that<sup>59</sup> for a channel  $\Phi$  that is covariant under a unitary representation of some group  $G$ , i.e.

$$\Phi(\hat{U}_g^A \hat{\rho} \hat{U}_g^{A\dagger}) = \hat{U}_g^B \Phi(\hat{\rho}) \hat{U}_g^{B\dagger}, \quad \forall \hat{\rho} \in \mathfrak{E}(\mathcal{H}), \forall g \in G, \quad (68)$$

then also the complementary channel  $\tilde{\Phi}$  is covariant under the same transformations, i.e.

$$\tilde{\Phi}(\hat{U}_g^A \hat{\rho} \hat{U}_g^{A\dagger}) = \hat{U}_g^E \tilde{\Phi}(\hat{\rho}) \hat{U}_g^{E\dagger}, \quad \forall \hat{\rho} \in \mathfrak{E}(\mathcal{H}), \forall g \in G, \quad (69)$$

where for  $X = A, B, E$ ,  $\hat{U}_g^X$  is the unitary operator that represents the element  $g$  of the group  $G$  in the output space  $X$ .

We finally recall the definition of degradable and anti-degradable channels<sup>48</sup>. A quantum channel  $\Phi$  is said degradable if a CPTP map  $\mathcal{N} : \mathcal{L}(\mathcal{H}_B) \rightarrow \mathcal{L}(\mathcal{H}_E)$  exists s.t.

$$\tilde{\Phi} = \mathcal{N} \circ \Phi, \quad (70)$$

while it is said antidegradable if it exists a CPTP map  $\mathcal{M} : \mathcal{L}(\mathcal{H}_E) \rightarrow \mathcal{L}(\mathcal{H}_B)$  s.t.

$$\Phi = \mathcal{M} \circ \tilde{\Phi}, \quad (71)$$

(the symbol “ $\circ$ ” representing channel concatenation). Notice that in case  $\Phi$  is mathematically invertible, a simple direct way to determine whether it is degradable or not is to formally invert Eq. (70) constructing the super-operator  $\tilde{\Phi} \circ \Phi^{-1}$  and check whether such object is CPTP (e.g. by studying the positivity of its Choi matrix)<sup>60,61</sup>, i.e. explicitly

$$\Phi \text{ invertible} \Rightarrow \Phi \text{ degradable iff } \tilde{\Phi} \circ \Phi^{-1} \text{ is CPTP.} \quad (72)$$

Concretely this can be done by using the fact that since quantum channels are linear maps connecting vector spaces of linear operators, they can in turn be represented as matrices acting on vector spaces. This through the following vectorization isomorphism:

$$\begin{aligned} \hat{\rho}_A &= \sum_{ij} \rho_{ij} |i\rangle\langle j|_A \otimes |j\rangle\langle i|_A \in \mathcal{H}_A^{\otimes 2} \\ \Phi(\hat{\rho}_A) &\longmapsto \hat{M}_\Phi |\rho\rangle, \end{aligned} \quad (73)$$

where now  $\hat{M}_\Phi$  is a  $d_B^2 \times d_A^2$  matrix connecting  $\mathcal{H}_A^{\otimes 2}$  and  $\mathcal{H}_B^{\otimes 2}$  ( $d_A$  and  $d_B$  being, respectively, the dimensions of  $\mathcal{H}_A$  and  $\mathcal{H}_B$ ), which given a Kraus set  $\{\hat{M}_k\}_k$  for  $\Phi$  it can be explicitly expressed as

$$\hat{M}_\Phi = \sum_k \hat{M}_k \otimes \hat{M}_k^*. \quad (74)$$

Following Eq. (70), we have, hence, that for a degradable channel the following

identity must apply

$$\hat{M}_{\tilde{\Phi}} = \hat{M}_\Phi \hat{M}_\Phi^*, \quad (75)$$

with  $\hat{M}_\Phi$  the matrix representation of the CPTP connecting channel  $\mathcal{N}$ , implying that the super-operator  $\tilde{\Phi} \circ \Phi^{-1}$  is now represented by matrix  $\hat{M}_{\tilde{\Phi}} \hat{M}_\Phi^{-1}$ .

**Covariance of the channel.** Besides allowing for the single-letter simplification in Eq. (15), another important consequence of the degradability property of Eq. (70) is the fact that, for channels fulfilling such condition, the coherent information in Eq. (11) is known to be concave<sup>62</sup> with respect to the input state  $\hat{\rho}$ , i.e.

$$J\left(\Phi, \sum_k p_k \hat{\rho}_k\right) \geq \sum_k p_k J(\Phi, \hat{\rho}_k), \quad (76)$$

for all statistical ensemble of input states  $\{p_k; \hat{\rho}_k\}$ . This last inequality allows for some further drastic simplification in particular when the channel  $\Phi$  is covariant under a group of unitary transformations as in Eq. (68). Indeed, thanks to ref. <sup>59</sup> and the invariance of the von Neumann entropy under unitary operations, we can now observe that

$$\begin{aligned} J(\Phi, \hat{U}_g^A \hat{\rho} \hat{U}_g^{A\dagger}) &= S(\Phi(\hat{U}_g^A \hat{\rho} \hat{U}_g^{A\dagger})) - S(\tilde{\Phi}(\hat{U}_g^A \hat{\rho} \hat{U}_g^{A\dagger})) \\ &= S(\hat{U}_g^B \Phi(\hat{\rho}) \hat{U}_g^{B\dagger}) - S(\hat{U}_g^E \tilde{\Phi}(\hat{\rho}) \hat{U}_g^{E\dagger}) \\ &= J(\Phi, \hat{\rho}), \end{aligned} \quad (77)$$

for all input states and for all elements  $g$  of the group. Given then a generic input state  $\hat{\rho}$  of the system, construct the following ensemble of density matrices  $\{d\mu(g); \hat{\rho}_g\}$  with  $d\mu(g)$  some properly defined probability distribution on  $G$  and with  $\hat{\rho}_g \equiv \hat{U}_g^A \hat{\rho} \hat{U}_g^{A\dagger}$ . Defining then

$$\Lambda_G[\hat{\rho}] \equiv \int d\mu_g \hat{\rho}_g = \int d\mu_g \hat{U}_g^A \hat{\rho} \hat{U}_g^{A\dagger}, \quad (78)$$

the average state of  $\{d\mu(g); \hat{\rho}_g\}$  we notice that if  $\Phi$  is degradable the following inequality holds true:

$$J(\Phi, \Lambda_G[\hat{\rho}]) \geq \int d\mu_g J(\Phi, \hat{U}_g^A \hat{\rho} \hat{U}_g^{A\dagger}) = J(\Phi, \hat{\rho}), \quad (79)$$

where in the last passage we used the invariance in Eq. (77). Accordingly, we can now restrict the maximization in Eq. (9) to only those input states  $\hat{\rho}_G$  which result from the averaging operation of Eq. (78), i.e.

$$Q(\Phi) = Q^{(1)}(\Phi) = \max_{\hat{\rho}_G} J(\Phi, \hat{\rho}_G). \quad (80)$$

For the special case of the MAD channels  $\mathcal{D}$  introduced in “Methods”—(MAD channels and composition rules), thanks to Eq. (4) we can identify the group  $G$  with the set of unitary operations which are diagonal in the computational basis  $\{|i\rangle\}_{i=0, \dots, d-1}$ . Taking  $d\mu_g$  a flat measure, Eq. (78) allows us to identify  $\Lambda_G[\hat{\rho}]$  with the density matrices of  $A$  which are diagonal as well, i.e.

$$\Lambda_G[\hat{\rho}] = \text{diag}[\hat{\rho}], \quad (81)$$

and therefore to derive from Eq. (80) the following compact expression:

$$Q(\mathcal{D}) = Q^{(1)}(\mathcal{D}) = \max_{\hat{\rho}_{\text{diag}}} J(\mathcal{D}, \hat{\rho}_{\text{diag}}), \quad (82)$$

which for  $d_C = 3$  reduces to Eq. (16) of the main text. For completeness, we report also an alternative, possibly more explicit way to derive Eq. (82). This is obtained by observing that a special instance of the unitaries which are diagonal in the computational basis of a MAD channel and hence fulfill the identity in Eq. (4), is provided by the subgroup  $\mathcal{O}_D(d)$  formed by the operators represented by the diagonal  $d \times d$  matrices for which all the non-zero (and diagonal) elements are  $\pm 1$ . Clearly the identity operator  $\hat{1}$  is an element of  $\mathcal{O}_D(d)$  and the group is finite with  $2^d$  elements. Given then an arbitrary input state  $\hat{\rho}$  of  $A$ , construct then the ensemble  $\{p_k; \hat{\rho}_k\}$  formed by the density matrices  $\hat{\rho}_k \equiv \hat{O}_k \hat{\rho} \hat{O}_k^\dagger$ , with  $\hat{O}_k$  being the  $k$ -th element of  $\mathcal{O}_D(d)$ , and by a flat probability set  $p_k = 1/2^d$ . It can be shown<sup>63</sup> that the average state of  $\{p_k; \hat{\rho}_k\}$  is diagonal in the computational basis, i.e.

$$\frac{1}{2^d} \sum_{k=0}^{2^d-1} \hat{O}_k \hat{\rho} \hat{O}_k^\dagger = \text{diag}(\hat{\rho}), \quad (83)$$

from which Eq. (82) can once more be derived as a consequence of Eq. (80) for all degradable  $\mathcal{D}$ .

### Data availability

Data used to produce the figures shown in the manuscript are available from the corresponding author upon request.

Received: 29 August 2020; Accepted: 5 January 2021;

Published online: 10 February 2021

## References

- Shannon, C. E. A mathematical theory of communication. *Bell Syst. Tech. J.* **27**, 379–423 (1948).
- Holevo, A. S. & Giovannetti, V. Quantum channels and their entropic characteristics. *Rep. Prog. Phys.* **75**, 4 (2012).
- Bennett, C. H. & Shor, P. W. Quantum information theory. *IEEE Trans. Inform. Theory* **44**, 2724 (1998).
- Holevo, A. S. *Quantum Systems, Channels, Information* (De Gruyter, 2019).
- Wilde, M. *Quantum Information Theory* (Cambridge University Press, 2017).
- Watrous, J. *The Theory of Quantum Information* (Cambridge University, 2018).
- Nielsen, M. & Chuang, I. *Quantum Computation and Quantum Information: 10th Anniversary Edition* 10th edn (Cambridge University Press, 2011).
- Gyongyosi, L., Imre, S. & Nguyen, H. V. A survey on quantum channel capacities. *IEEE Commun. Surv. Tutor.* **20**, 1149–1205 (2018).
- Giovannetti, V. & Fazio, R. Information-capacity description of spin-chain correlations. *Phys. Rev. A* **71**, 032314 (2005).
- D’Arrigo, A., Benenti, G., Falci, G. & Macchiavello, C. Classical and quantum capacities of a fully correlated amplitude damping channel. *Phys. Rev. A* **88**, 042337 (2013).
- Jahangir, R., Arshed, N. & Toor, A. H. Quantum capacity of an amplitude-damping channel with memory. *Quantum Inf. Process.* **14**, 765–782 (2015).
- D’Arrigo, A., Benenti, G., Falci, G. & Macchiavello, C. Information transmission over an amplitude damping channel with an arbitrary degree of memory. *Phys. Rev. A* **92**, 062342 (2015).
- Ouyang, Y. Channel covariance, twirling, contraction, and some upper bounds on the quantum capacity. *Quantum Inf. Comput.* **14**, 0917–0936 (2014).
- Macchiavello, C. & Sacchi, M. F. Efficient accessible bounds to the classical capacity of quantum channels. *Phys. Rev. Lett.* **123**, 090503 (2019).
- Muthukrishnan, A. & Stroud, C. R. Multivalued logic gates for quantum computation. *Phys. Rev. A* **62**, 052309 (2000).
- Lanyon, B. et al. Simplifying quantum logic using higher-dimensional Hilbert spaces. *Nat. Phys.* **5**, 134–140 (2009).
- Ralph, T. C., Resch, K. J. & Gilchrist, A. Efficient Toffoli gates using qudits. *Phys. Rev. A* **75**, 022313 (2007).
- Ivanov, S. S., Tonchev, H. S. & Vitanov, N. V. Time-efficient implementation of quantum search with qudits. *Phys. Rev. A* **85**, 062321 (2012).
- Gedik, Z. et al. Computational speed-up with a single qudit. *Sci. Rep.* **5**, 14671 (2015).
- Kiktenko, E. O., Nikolaeva, A. S., Xu, P., Shlyapnikov, G. V. & Fedorov, A. K. Scalable quantum computing with qudits on a graph. *Phys. Rev. A* **101**, 022304 (2020).
- Cozzolino, D., DaLio, B., Bacco, D. & Oxenlowe, L. K. High-dimensional quantum communication: benefits, progress, and future challenges. *Adv. Quantum Technol.* **2**, 1900038 (2019).
- Looi, S. Y., Yu, L., Gheorghiu, V. & Griffiths, R. B. Quantum-error-correcting codes using qudit graph states. *Phys. Rev. A* **78**, 042303 (2008).
- Goyal, S. K., Boukama-Dzoussi, P. E., Ghosh, S., Roux, F. S. & Konrad, T. Qudit-teleportation for photons with linear optics. *Sci. Rep.* **4**, 4543 (2014).
- Muralidharan, S., Zou, C.-L., Li, L., Wen, J. & Jiang, L. Overcoming erasure errors with multilevel systems. *New J. Phys.* **19**, 013026 (2017).
- Lima, G. et al. Experimental quantum tomography of photonic qudits via mutually unbiased basis. *Opt. Express* **19**, 3542–3552 (2011).
- Nisbet-Jones, P. et al. Photonic qubits, qutrits and ququads accurately prepared and delivered on demand. *New J. Phys.* **15**, 053007 (2013).
- Marques, B. et al. Experimental simulation of decoherence in photonics qudits. *Sci. Rep.* **5**, 16049 (2015).
- Babazadeh, A. et al. High-dimensional single-photon quantum gates: concepts and experiments. *Phys. Rev. Lett.* **119**, 180510 (2017).
- Kues, M. et al. On-chip generation of high-dimensional entangled quantum states and their coherent control. *Nature* **546**, 622–626 (2017).
- Moreno-Pineda, E. et al. Molecular spin qudits for quantum algorithms. *Chem. Soc. Rev.* **47**, 501–513 (2018).
- Giordani, T. et al. Experimental engineering of arbitrary qudit states with discrete-time quantum walks. *Phys. Rev. Lett.* **122**, 020503 (2019).
- Sawant, R. et al. Ultracold polar molecules as qudits. *New J. Phys.* **22**, 013027 (2020).
- Chessa, S. & Giovannetti, V. Partially coherent direct sum channels. Preprint at <https://arxiv.org/abs/2008.00494> (2020).
- Brußand, D. & Macchiavello, C. Optimal eavesdropping in cryptography with three-dimensional quantum states. *Phys. Rev. Lett.* **88**, 127901 (2002).
- Klimov, A. B., Guzmán, R., Retamal, J. C. & Saavedra, C. Qutrit quantum computer with trapped ions. *Phys. Rev. A* **67**, 062313 (2003).
- Kaszlikowsky, D. et al. Quantum cryptography based on qutrit Bell inequalities. *Phys. Rev. A* **67**, 012310 (2003).
- Bartůšková, L. et al. Optical implementation of the encoding of two qubits to a single qutrit. *Phys. Rev. A* **74**, 022325 (2006).
- Lanyon, B. P. et al. Manipulating biphotonic qutrits. *Phys. Rev. Lett.* **100**, 060504 (2008).
- Bocharov, A., Roetteler, M. & Svore, K. M. Factoring with qutrits: Shor’s algorithm on ternary and metaplectic quantum architectures. *Phys. Rev. A* **96**, 012306 (2017).
- Shlyakhov, A. R. et al. Quantum metrology with a transmon qutrit. *Phys. Rev. A* **97**, 022115 (2018).
- Luo, Y.-H. et al. Quantum teleportation in high dimensions. *Phys. Rev. Lett.* **123**, 070505 (2019).
- Bækkegaard, T. B. et al. Realization of efficient quantum gates with a superconducting qubit-qutrit circuit. *Sci. Rep.* **9**, 13389 (2019).
- Li, B., Yu, Z. & Fei Geometry of quantum computation with qutrits. *Sci. Rep.* **3**, 2594 (2013).
- Lloyd, S. Capacity of the noisy quantum channel. *Phys. Rev. A* **55**, 1613 (1997).
- Shor, P. W. The quantum channel capacity and coherent information. *Lecture Notes, MSRI Workshop on Quantum Computation (Quantum Information and Cryptography)* <https://www.msri.org/workshops/203/schedules/1181> (2002).
- Devetak, I. The private classical capacity and quantum capacity of a quantum channel. *IEEE Trans. Inform. Theory* **51**, 44–55 (2005).
- Cai, N., Winter, A. & Yeung, R. W. Quantum privacy and quantum wiretap channels. *Probl. Inf. Transm.* **40**, 318–336 (2004).
- Devetak, I. & Shor, P. W. The capacity of a quantum channel for simultaneous transmission of classical and quantum information. *Math. Phys.* **256**, 287–303 (2005).
- Caruso, F. & Giovannetti, V. Degradability of Bosonic Gaussian channels. *Phys. Rev. A* **74**, 062307 (2006).
- Smith, G. The private classical capacity with a symmetric side channel and its application to quantum cryptography. *Phys. Rev. A* **78**, 022306 (2008).
- Keyl, M. Fundamentals of quantum information theory. *Phys. Rep.* **369**, 431 (2002).
- Khatiri, S., Sharma, K. & Wilde, M. M. Information-theoretic aspects of the generalized amplitude-damping channel. *Phys. Rev. A* **102**, 012401 (2020).
- Cubitt, T., Ruskai, M. & Smith, G. The structure of degradable quantum channels. *J. Math. Phys.* **49**, 102104 (2008).
- Bennett, C. H., Shor, P. W., Smolin, J. A. & Thapliyal, A. V. Entanglement-assisted classical capacity of noisy quantum channels. *Phys. Rev. Lett.* **83**, 3081 (1999).
- Bennett, C. H., Shor, P. W., Smolin, J. A. & Thapliyal, A. V. Entanglement-assisted capacity of a quantum channel and the reverse Shannon theorem. *IEEE Trans. Inform. Theory* **48**, 2637–2655 (2002).
- Pirandola, S., Laurenza, R., Ottaviani, C. & Banchi, L. Fundamental limits of repeaterless quantum communications. *Nat. Commun.* **8**, 15043 (2017).
- Choi, M. D. Completely positive linear maps on complex matrices. *Linear Algebra Appl.* **10**, 285–290 (1975).
- Stinespring, W. Positive functions on  $C^*$ -algebras. *Proc. Am. Math. Soc.* **6**, 211–216 (1955).
- Holevo, A. Complementary channels and the additivity problem. *Theory Probab. Appl.* **51**, 92–100 (2007).
- Smith, G. & Smolin, J. Degenerate quantum codes for Pauli channels. *Phys. Rev. Lett.* **98**, 030501 (2007).
- Wolf, M. & Perez-Garcia, D. Quantum capacities of channels with small environment. *Phys. Rev. A* **75**, 012303 (2007).
- Yard, J., Hayden, P. & Devetak, I. Capacity theorems for quantum multiple-access channels: classical-quantum and quantum-quantum capacity regions. *IEEE Trans. Inform. Theory* **54**, 3091–3113 (2008).
- Servaes. Effect of diagonal orthogonal matrices (version: 2018-12-12). <https://math.stackexchange.com/q/3036627> (2018).

## Acknowledgements

We acknowledge support from PRIN 2017 “Taming complexity with quantum strategies”. S.C. thanks P. Novelli for fruitful discussions.

## Author contributions

S.C. and V.G. contributed equally to the conception and writing of the manuscript.

**Competing interests**

The authors declare no competing interests.

**Additional information**

**Supplementary information** The online version contains supplementary material available at <https://doi.org/10.1038/s42005-021-00524-4>.

**Correspondence** and requests for materials should be addressed to S.C.

**Reprints and permission information** is available at <http://www.nature.com/reprints>

**Publisher's note** Springer Nature remains neutral with regard to jurisdictional claims in published maps and institutional affiliations.



**Open Access** This article is licensed under a Creative Commons Attribution 4.0 International License, which permits use, sharing, adaptation, distribution and reproduction in any medium or format, as long as you give appropriate credit to the original author(s) and the source, provide a link to the Creative Commons license, and indicate if changes were made. The images or other third party material in this article are included in the article's Creative Commons license, unless indicated otherwise in a credit line to the material. If material is not included in the article's Creative Commons license and your intended use is not permitted by statutory regulation or exceeds the permitted use, you will need to obtain permission directly from the copyright holder. To view a copy of this license, visit <http://creativecommons.org/licenses/by/4.0/>.

© The Author(s) 2021